

UVES observations of a damped Ly α system at $z_{\text{abs}} = 4.466$ towards the quasar APM BR J0307–4945^{*}

M. Dessauges-Zavadsky^{1,2}, S. D’Odorico¹, R.G. McMahon³, P. Molaro⁴, C. Ledoux¹, C. Péroux³ and L.J. Storrie-Lombardi⁵

¹ European Southern Observatory, Karl-Schwarzschildstr. 2, 85748 Garching bei München, Germany

² Observatoire de Genève, 1290 Sauverny, Switzerland

³ Institute of Astronomy, Madingley Road, Cambridge CB3 0HA, England

⁴ Osservatorio Astronomico di Trieste, Via G.B. Tiepolo 11, 34131 Trieste, Italy

⁵ SIRTf Science Center, California Institute of Technology, MS 100-22, Pasadena, CA, USA

Received / Accepted

Abstract. We present the first high-resolution (6.2 to 7.7 km s⁻¹ FWHM) spectra of the APM BR J0307–4945 quasar at $z_{\text{em}} = 4.73$ obtained with UVES on the 8.2m VLT Kueyen telescope. We focus our analysis on a damped Ly α (DLA) system at $z_{\text{abs}} = 4.466$ with a neutral hydrogen column density $N(\text{H I}) = (4.68 \pm 0.97) \cdot 10^{20} \text{ cm}^{-2}$. It is the most distant DLA system known to the present date, observed when the age of the universe was only 1.3 Gyr. It shows complex low- and high-ionization line profiles spanning ≈ 240 and 300 km s⁻¹ in velocity space respectively. We derive accurate abundances for N, O, Al, Si and Fe, and place a lower limit on C and an upper limit on Ni: $[\text{N}/\text{H}] = -3.07 \pm 0.15$, $[\text{O}/\text{H}] = -1.63 \pm 0.19$, $[\text{Al}/\text{H}] = -1.79 \pm 0.11$, $[\text{Si}/\text{H}] = -1.54 \pm 0.11$, $[\text{Fe}/\text{H}] = -1.97 \pm 0.19$, $[\text{C}/\text{H}] > -1.63$ and $[\text{Ni}/\text{H}] < -2.35$. The derived high metallicity, $\sim 1/90$ solar, shows that this very young absorber (≤ 1.3 Gyr) has already experienced a significant metal enrichment. The $[\text{O}/\text{Si}]$ ratio is nearly solar suggesting a limited amount of dust, the relative $[\text{Si}, \text{O}/\text{Fe}]$ abundance ratios show a similar enhancement as observed in the Milky Way stars with comparable metallicities, and the $[\text{N}/\text{O}]$ ratio is very low. All these results point to an enrichment pattern dominated by Type II supernovae which suggests a Milky Way type evolutionary model.

Key words: Cosmology: observations – Galaxies: abundances – Galaxies: evolution – Quasars: absorption lines

1. Introduction

For two decades now bright quasars (hereafter QSOs) have been used to investigate the distribution and physical properties of gas in their lines of sight up to their emission redshift. The information is extracted from the study of

absorption lines originating in the gas (the Hydrogen Lyman series lines and resonance lines of various metal ions) as detected in the high dispersion ($10000 < R < 50000$) spectra of the QSOs.

A special class of absorption systems is represented by the damped Ly α systems. DLA systems are defined as absorption systems with a H I column density $\geq 2 \cdot 10^{20} \text{ cm}^{-2}$ which gives origin to the characteristic damped profile in the Ly α absorption. There is no general consensus on the nature of the galaxies associated with the DLA systems. The identification of all DLA systems with progenitors of present-day spirals as proposed originally by Wolfe et al. (1986) is not fully supported by the observations of optical counterparts at low redshifts which show a variety of morphological types (e.g. Le Brun et al. 1997) and by the relative metal abundances.

Whatever their nature, DLA systems appear to be associated with the bulk of neutral hydrogen in the universe at high redshift (Wolfe et al. 1995, Lanzetta et al. 1995, Storrie-Lombardi et al. 1996) and remain a unique way to trace accurately chemical abundances over a wide interval of redshifts, from 0.5 to 4.5, setting important constraints on theories of galaxy formation and evolution.

In the last decade, this type of research has especially benefitted from the use of the HIRES spectrograph at the Keck telescope. HIRES observations have produced a large number of accurate abundance measurements in DLA systems (Lu et al. 1996, 1997, Prochaska & Wolfe 1999) which together with more complete DLA surveys (Rao & Turnshek 2000, Storrie-Lombardi & Wolfe 2000) have been used to explore both the redshift evolution of comoving mass density and of the metal content (see for a recent review Pettini 2000). It is unclear whether any of these quantities is significantly evolving from the early universe ($\sim 10\%$ of the present age) to the present epoch, in contradiction with the simple picture describing a progressive conversion of gas into stars and an increase in the mean metallicity. Indeed, DLA systems at all redshifts

Send offprint requests to: mdessaug@eso.org

^{*} Based on public data released from UVES Commissioning at the VLT/Kueyen telescope, ESO, Paranal, Chile.

Table 1. Journal of observations

Number of spectra	Date	Central wavelength [Å]	Range [Å]	Resolution $\lambda/\Delta\lambda_{\text{instr.}}$	CD grating	Slit width ["]	Seeing ["]	Exposure time [s]
1	13/10/99	6000	5000–5960	39020	#3	1.1	0.8	4400
3	8/10/99	7600	6120–7000	38980	#4	1.0	0.7–0.9	3300/3000/3300
3	14/12/99	8000	5800–7500	43880	#4	0.9	0.8	4000/4000/4300
			7710–9510	43550				
			6120–7960	48020				
			8100–9900	46090				

Mode: mosaic of the RED arm.

might simply represent galaxies “caught in the act” of assembling a large amount of gas before a major episode of star formation.

Whatever the favorite interpretation, it is clear that the sample of DLA systems with high-quality spectroscopic data (now summing up to about 70 objects) has to be substantially enlarged, to increase the statistical weight of the results at all redshifts and in particular at the low and very high redshift ends. The number of well studied systems at high redshifts is particularly low. The recent overview of abundance determinations by Prochaska & Wolfe (2000) includes 13 objects at $z_{\text{abs}} \geq 3$ and 5 objects at $z_{\text{abs}} \geq 4$ only.

In October 1999, ESO installed at the second 8.2m VLT telescope (Kueyen) its high-resolution spectrograph, UVES, which compares well in efficiency and resolution with HIRES (D’Odorico et al. 2000). Taking advantage of its superior near-infrared efficiency, UVES has already been used to secure the first Zn abundance in a DLA system at $z_{\text{abs}} > 3$ so far (Molaro et al. 2000).

In this paper we report UVES observations of the highest redshift ($z_{\text{abs}} = 4.466$) DLA system known to the present date. The quality of the data is such that a detailed analysis of the metal content of the absorbing gas has been possible and from this the evolutionary history of the associated galaxy has been reconstructed. While the statistical weight of the results on a single DLA system is obviously limited, with this study we demonstrate the possibility to investigate the star formation history of galaxies well beyond $z = 4$ from observations of relatively faint QSOs. The observations were obtained during the Commissioning of the instrument. They are part of the public set of UVES Commissioning data available through the ESO VLT archive.

In Sect. 2 we briefly review the observations and data reduction, and we provide a list of all metal systems we have identified in the line of sight to APM BR J0307–4945 redwards of the Ly α emission. We report the column density measurements of different ions of the DLA system at $z_{\text{abs}} = 4.466$ in Sect. 3. Sect. 4 discusses the abundances and Sect. 5 the kinematics of the DLA gas. The conclusions are summarized in Sect. 6.

2. Data

2.1. Observations

APM BR J0307–4945 is a newly discovered quasar at $z_{\text{em}} = 4.73$ ($R = 18.8$) from the second APM color survey for $z > 4$ QSOs (Storrie-Lombardi et al. 2001). The damped absorber at $z_{\text{abs}} = 4.466$ was so prominent that it was identifiable in the low resolution (FWHM ~ 10 Å) quasar discovery spectrum. On the basis of medium resolution spectroscopy (FWHM ~ 5 Å) the DLA column density was estimated to be $\log N(\text{H I}) = 20.8$ (Péroux et al. 2001 and McMahon et al. 2001, in preparation).

The observations of APM BR J0307–4945 presented here were obtained during the first and second Commissioning of the Ultraviolet-Visual Echelle Spectrograph (UVES) on the Nasmyth focus of the VLT 8.2m Kueyen telescope at Paranal, in October and December 1999. A journal of observation dates, wavelength coverages, resolutions and exposure times of the data is presented in Table 1. Seven spectra, covering in total the spectral range from 5000 to 9900 Å, were obtained by using the cross-disperser gratings #3 and #4 of the spectrograph red arm. Details on the instrument can be found in Dekker et al. (2000) and in the UVES User Manual available at <http://www.eso.org/instruments/uves/userman/>. The full width at half maximum of the instrument profile, $\Delta\lambda_{\text{instr.}}$, was measured from the emission lines of the Thorium-Argon lamp and the resulting resolving powers, $R = \lambda/\Delta\lambda_{\text{instr.}}$, vary between 38980 and 48020 (median values) depending on the spectra (see Table 1) and correspond to a velocity resolution of 6.2 to 7.7 km s $^{-1}$ FWHM.

2.2. Data reduction

The data reduction was performed on each of the seven spectra separately using the UVES data reduction pipeline implemented in the ESO MIDAS package. The pipeline reduction is based on the following steps: order definition using a special order definition frame (order width $\simeq 5$ pixels); wavelength calibration; order extraction using the “optimal” extraction method (the orders are extracted by calculating a weighted sum of pixel values across the pro-

file of the object); extraction of weighted flat-field; flat-fielding; and sky subtraction. Typical RMS errors in the wavelength calibrations are ≤ 5.5 mÅ.

The observed wavelength scale was transformed into vacuum, heliocentric scale. The spectra were normalized by using a spline to smoothly connect the regions free from absorption features. The continuum for the Ly α forest region was fitted by using small regions deemed to be free of absorptions and by interpolating between these regions with a spline. Finally, the normalized spectra were added together using their S/N as weights. The final spectrum reaches a signal-to-noise of $20 \leq S/N \leq 40$.

2.3. Absorption line identification

We have proceeded with the absorption-line identification by first trying to find all C IV, Si IV and Mg II doublets. Once we had composed a list of redshifts for the metal-line systems, we attempted to match the remaining absorption features with the strongest metal-line transitions. Finally, we compared in velocity space the line profiles of individual transitions in the determined systems for conclusive identification. The discrimination of telluric absorption lines from extragalactic absorption has been possible thanks to the spectrum of a standard star covering the spectral ranges from 6120 to 7960 Å and from 8100 to 9900 Å, and the comparison of spectra taken at different epochs.

Table 5¹ lists the wavelengths and equivalent widths for all absorption-line features (except the telluric lines) redwards of the Ly α emission that exceed the 4σ limit in equivalent width. The transition names and approximate redshifts are specified for the features we successfully identified. About 80% of the absorption lines redwards of the Ly α emission have been identified, corresponding to 13 metal-line systems. In this work we will restrict our analysis to the damped Ly α system at $z_{\text{abs}} = 4.466$.

3. Ionic column densities

We present here the measurements of ionic column densities obtained for the damped Ly α system at $z_{\text{abs}} = 4.466$. They have been derived by fitting theoretical Voigt profiles to the observed absorption lines via a χ^2 minimization. The fits were performed using the FITLYMAN package included in MIDAS (Fontana & Ballester 1995). During the fitting procedure the theoretical profiles were convolved with the instrumental point spread function modeled from the analysis of the emission lines of the arcs. The FITLYMAN routines determine for each absorption component the redshift, the column density, the turbulent broadening parameter b and the fit errors for each of these quantities. The atomic data are taken from the compilation of Morton (1991) and from the updated values of Spitzer &

Fitzpatrick (1993) for silicon, Cardelli & Savage (1995) for iron and Zsargó & Federman (1998) for nickel, as specified in Table 4.

The velocity profiles and the best fitting solutions of the low-ion transitions (C⁺, N⁰, O⁰, Al⁺, Si⁺ and Fe⁺) associated with the damped Ly α system at $z_{\text{abs}} = 4.466$ are plotted in Fig. 1. The velocity centroids for the different components of the fit are marked by the short vertical lines. To obtain these fitting solutions, we assumed the same b -values in the same component of all ions (i.e. that macroturbulent motions dominate over thermal broadening) and the same redshift, and allowed for variations from ion to ion in column density only. We find that a minimum of twelve components was required to fit the low-ion transitions. The stronger components are the components 7, 8 (at $z = 4.466582$, $z = 4.466844$) and the components 10, 11 (at $z = 4.467863$, $z = 4.468005$). Table 2 lists the redshift, the b -value and the column density of every velocity component of the fitting solution.

The velocity profiles and the best fitting solutions for the high-ion transitions (C³⁺ and Si³⁺ partly blended by the telluric absorption lines), which were obtained independently from the low-ion transitions, are given in Fig. 2 and in Table 3. A total of fourteen components were required to fit the high-ion transitions, with the dominant one lying at $z = 4.465953$ (component 8).

3.1. Hydrogen content

The hydrogen column density was mainly estimated from the fit of the Ly α damping profile. The main difficulty of the Ly α profile fitting in this DLA system, as is often the case at high redshift, is the strong contamination by Ly α forest lines on both wings of the damped Ly α line. The Ly β and Ly γ lines are heavily blended and thus unusable for a hydrogen column density determination, unlike the Ly δ line.

Fits provided by the Ly α and Ly δ lines by taking into account only one of the four stronger components of the low-ion fits (component 7, nearly centered on the Ly α and Ly δ profiles), yield a satisfactory result only to the blue side of the Ly α profile (the Ly δ blue side profile is contaminated by the Ly α forest absorptions). However, they leave an “empty space” on the red side on each of these two line profiles, which can be filled by adding the contribution of the second dominant component, the component 11 (see Fig. 3).

The corresponding hydrogen column densities and b -values are $\log N(\text{H I}) = 20.03$, $b = 20.0$ km s⁻¹ for the component 7 at $z = 4.466582$ and $\log N(\text{H I}) = 20.56$, $b = 16.5$ km s⁻¹ for the component 11 at $z = 4.468005$. The b -value of the component 11 is constrained by the blue side of the Ly δ line. The resulting total hydrogen column density is $\log N(\text{H I}) = 20.67 \pm 0.09$.

The hydrogen column density value determined in the DLA system at $z_{\text{abs}} = 4.466$ is consistent with the lack

¹ Available in electronic form at <http://cdsweb.u-strasbg.fr>

Table 2. Fits for the DLA system at $z_{\text{abs}} = 4.466$ - Low-ions

Comp	z_{abs}	b [km s $^{-1}$]	Ident	$\log N$ [cm $^{-2}$]	Comp	z_{abs}	b [km s $^{-1}$]	Ident	$\log N$ [cm $^{-2}$]
1...	4.464386	13.5 ± 0.9	O I	13.12 ± 0.08	7...	4.466582	9.4 ± 3.5	O I	14.64 ± 0.70
			C II	13.58 ± 0.02				C II	> 13.95
			Si II	12.84 ± 0.11				Si II	13.61 ± 0.04
			Fe II	13.00 ± 0.21				Fe II	13.35 ± 0.25
			Al II	11.85 ± 0.07				Al II	11.59 ± 0.29
2...	4.464686	4.6 ± 0.2	N I	...	8...	4.466844	6.5 ± 1.3	N I	12.68 ± 0.30
			O I	13.59 ± 0.02				O I	14.61 ± 0.35
			C II	13.76 ± 0.04				C II	> 14.23
			Si II	13.17 ± 0.09				Si II	13.54 ± 0.02
			Fe II	12.80 ± 0.23				Fe II	12.69 ± 0.60
3...	4.465225	7.2 ± 2.1	Al II	11.93 ± 0.06	9...	4.467511	11.7 ± 1.6	Al II	12.15 ± 0.11
			N I	...				N I	12.70 ± 0.12
			O I	12.37 ± 0.35				O I	13.49 ± 0.04
			C II	13.13 ± 0.04				C II	13.25 ± 0.03
			Si II	12.57 ± 0.10				Si II	12.84 ± 0.07
4...	4.465510	6.2 ± 0.2	Fe II	12.72 ± 0.30	10...	4.467863	4.9 ± 0.8	Fe II	12.57 ± 0.44
			Al II	11.69 ± 0.09				Al II	11.77 ± 0.08
			N I	...				N I	...
			O I	14.02 ± 0.01				O I	15.33 ± 0.12
			C II	14.48 ± 0.04				C II	> 14.00
5...	4.465960	8.2 ± 0.5	Si II	13.67 ± 0.01	11...	4.468005	9.6 ± 0.3	Si II	13.57 ± 0.04
			Fe II	13.11 ± 0.13				Fe II	13.20 ± 0.13
			Al II	12.45 ± 0.04				Al II	12.05 ± 0.11
			N I	...				N I	12.84 ± 0.12
			O I	13.73 ± 0.02				O I	15.67 ± 0.14
6...	4.466417	14.4 ± 2.2	C II	> 14.43	12...	4.468343	4.4 ± 0.5	C II	> 15.42
			Si II	13.66 ± 0.02				Si II	14.14 ± 0.02
			Fe II	13.08 ± 0.14				Fe II	13.69 ± 0.05
			Al II	12.65 ± 0.04				Al II	12.61 ± 0.04
			N I	...				N I	13.30 ± 0.08
7...	4.466582	9.4 ± 3.5	O I	13.97 ± 0.13	13...	4.468343	4.4 ± 0.5	O I	14.17 ± 0.04
			C II	> 14.56				C II	13.16 ± 0.12
			Si II	13.97 ± 0.22				Si II	12.74 ± 0.06
			Fe II	13.21 ± 0.29				Fe II	12.64 ± 0.26
			Al II	12.77 ± 0.03				Al II	11.48 ± 0.13
8...	4.466844	6.5 ± 1.3	N I	...	14...	4.468343	4.4 ± 0.5	N I	...

of high neutral hydrogen column density DLA systems towards the highest redshifts (Storrie-Lombardi & Wolfe 2000). Indeed, in the sample described in the latter reference, 6 DLA absorbers out of 10 at $3 \leq z_{\text{abs}} \leq 3.5$ have $\log N(\text{HI}) > 21$, whereas the statistics drops to 1 out of 12 at $z_{\text{abs}} > 3.5$.

3.2. Metal abundances

The ionic column densities and the relative metal abundances of C, N, O, Al, Si, S, Fe and Ni measured for this DLA system at $z_{\text{abs}} = 4.466$ are summarized in Table 4. We give the total ionic column densities obtained by adding up all the components derived from the fits and their corresponding errors. The errors reflect the data quality and the errors on the b -values. The relative metal

abundances are estimated by assuming that the neutral and singly ionized species are associated with the neutral phase from which the HI column density originates and consequently do not require ionization corrections (Viegas 1995, Lu et al. 1995). Upper limits of detection are computed under the optically thin case approximation by considering the contributions of the four stronger components (7, 8, 10 and 11) not detected at 4σ . When the absorption lines are saturated, we give a lower limit.

The difficulty in determining accurate O I column densities is due to the fact that the only strong transition available redwards of the Ly α emission is the O I $\lambda 1302$ transition which is usually saturated in DLA systems. This transition is also saturated in this system at $z_{\text{abs}} = 4.466$ (see Fig. 1), and thus allows to derive only a lower limit to the total $N(\text{O I})$. We have looked for other oxygen

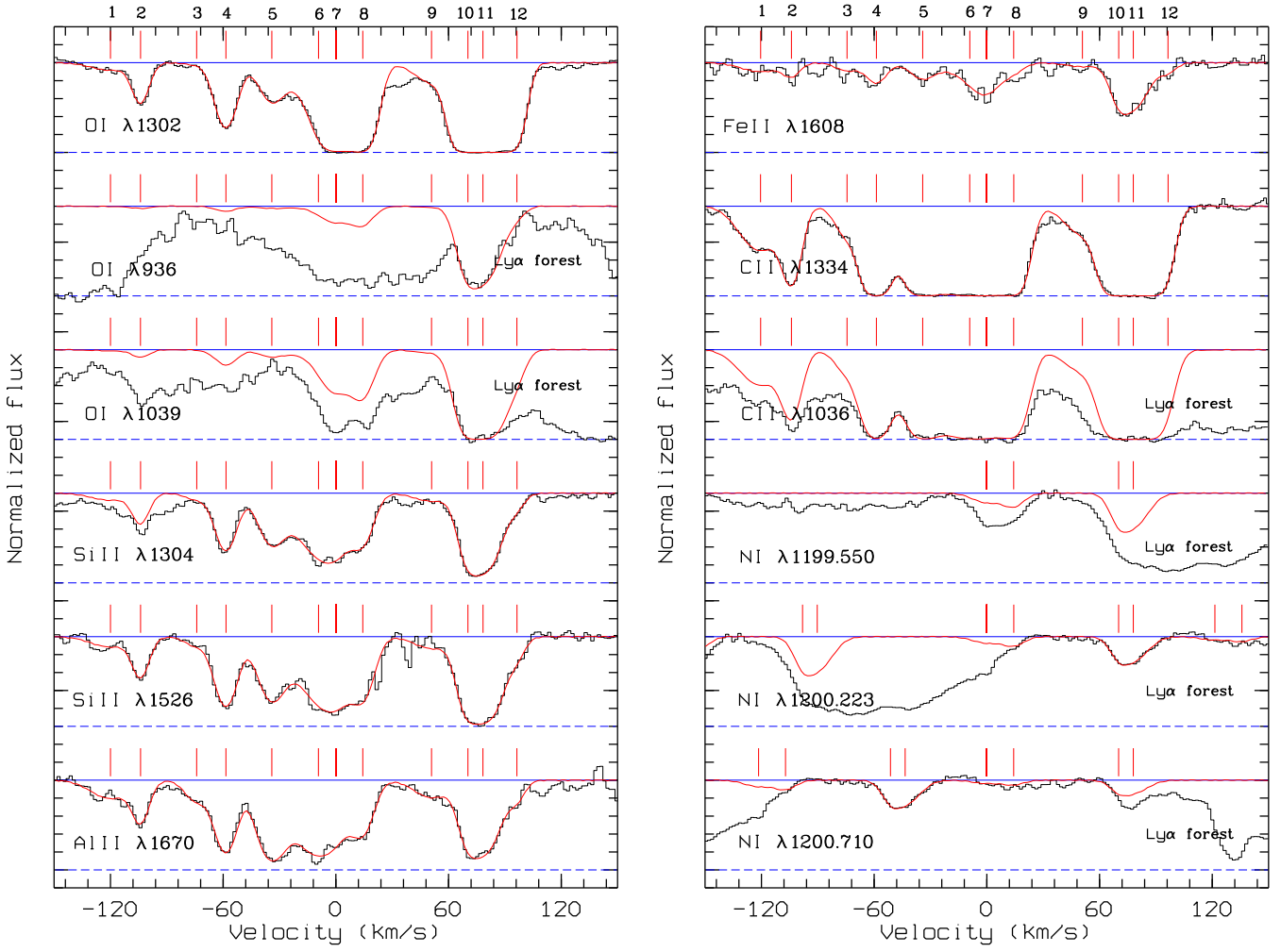


Fig. 1. Absorption-line profiles of the low-ion transitions plotted against velocity for the DLA system at $z_{\text{abs}} = 4.466$. The vertical scale goes from 0 to 1 for each plotted line transition. The zero velocity is fixed at $z = 4.466582$. The vertical bars mark the positions of the 12 velocity components given in Table 2. The thin solid curve represents the best fit solution. The Ni triplet is partly contaminated by the Ly α forest absorptions, thus the fit was performed only for their 4 stronger components (7, 8, 10 and 11).

lines in the Ly α forest namely, O I $\lambda 921.857$, $\lambda 929.517$, $\lambda 936.629$, $\lambda 948.685$, $\lambda 950.885$, $\lambda 988.773$ and $\lambda 1039.230$. Most of these lines are heavily contaminated by the Ly α forest absorption lines and cannot be used for any column density measurement. However, as we can see in Fig. 1, the O I $\lambda 936.629$ and $\lambda 1039.230$ lines put a stringent upper limit on the O I column densities of the two strong components 10 and 11, which are saturated in the O I $\lambda 1302$ line. This plays a crucial role in favour of the accuracy of the determined $N(\text{O I})$ column density value, since the measured upper limits are very close to the lower limit obtained from the O I $\lambda 1302$ line. Then, the only remaining saturated components in the O I $\lambda 1302$ line are the two other strong components 7 and 8 for which the other O I lines do not provide any constraint on their column densities. Nevertheless, the error made on the column densities

of these two components has a negligible effect on the total $N(\text{O I})$ column density: if we suppose a 40% underestimation of the column densities of the components 7 and 8 (which has an important impact on the fit quality of the O I $\lambda 1302$ line, owing to the very high signal-to-noise ratio in this region of the spectrum), it implies a variation of the total $\log N(\text{O I})$ of 0.02 only, a variation which is fully taken into account by the adopted error bar of 0.17 on $\log N(\text{O I})$. We conclude that the O I column density is constrained in the range $15.74 < \log N(\text{O I}) < 16.08$.

Accurate determinations of the carbon column densities present the same difficulty as for oxygen. The C II $\lambda 1334$ line redwards of the Ly α emission is heavily saturated and provides only a lower limit to $N(\text{C II})$, and the C II $\lambda 1036$ line is blended with Ly α forest absorptions (Fig. 1). The C II* $\lambda 1335$ metastable line is not detected,

Table 3. Fits for the DLA system at $z_{\text{abs}} = 4.466$ - High-ions

Comp	z_{abs}	b [km s $^{-1}$]	Ident	$\log N$ [cm $^{-2}$]	Comp	z_{abs}	b [km s $^{-1}$]	Ident	$\log N$ [cm $^{-2}$]
1...	4.463207	12.9 ± 6.0	C IV	12.61 ± 0.10	8...	4.465953	11.8 ± 2.2	C IV	13.72 ± 0.12
			Si IV	12.30 ± 0.14				Si IV	13.58 ± 0.22
2...	4.463557	12.1 ± 4.0	C IV	12.93 ± 0.05	9...	4.466476	10.8 ± 1.5	C IV	13.26 ± 0.03
			Si IV	12.62 ± 0.08				Si IV	13.24 ± 0.06
3...	4.463931	11.3 ± 2.2	C IV	13.13 ± 0.03	10...	4.466779	12.7 ± 5.4	C IV	12.78 ± 0.08
			Si IV	12.79 ± 0.05				Si IV	12.53 ± 0.06
4...	4.464331	4.7 ± 1.4	C IV	12.90 ± 0.05	11...	4.467173	19.0 ± 6.9	C IV	13.31 ± 0.03
			Si IV	12.79 ± 0.05				Si IV	13.14 ± 0.05
5...	4.464525	17.8 ± 6.1	C IV	13.09 ± 0.05	12...	4.467606	10.3 ± 1.9	C IV	13.13 ± 0.03
			Si IV	12.94 ± 0.05				Si IV	12.98 ± 0.04
6...	4.465333	19.8 ± 4.7	C IV	13.27 ± 0.03	13...	4.467994	5.1 ± 2.6	C IV	12.54 ± 0.07
			Si IV	12.89 ± 0.15				Si IV	12.45 ± 0.04
7...	4.465565	4.0 ± 1.8	C IV	12.72 ± 0.07	14...	4.468213	4.3 ± 3.5	C IV	12.42 ± 0.09
			Si IV	12.05 ± 0.21				Si IV	12.47 ± 0.04

and thus provides only an upper limit for the C II* column density.

Silicon has been derived from the Si II λ 1304 and λ 1526 lines and Al from the Al II λ 1670 line. The Ni II λ 1317 and λ 1370 lines are not detected, and thus provide only an upper limit for the Ni column density. The iron abundance is obtained from the Fe II λ 1608 line: $[\text{Fe}/\text{H}]^2 = -1.97 \pm 0.19$. Zn is a useful metal content indicator because it is undepleted in the interstellar medium (Pettini et al. 1997). Zn abundance measurements are however not possible in this DLA system, since the doublet Zn II λ 2026 and λ 2062 fall outside the working range of the spectrograph at an observed wavelength $\lambda > 11000 \text{ \AA}$.

The Ni I triplet near 1200 \AA is clearly detected (see Fig. 1) in the Ly α forest, although only the four stronger components (7, 8, 10 and 11) are free of the Ly α forest absorption contamination. By fitting these four components and by adding up their measured column densities, we derived a satisfactory value of the $N(\text{Ni I})$ column density (the contribution of the other eight components to the total column density is negligible compared to the contribution of these four dominant components). The S II triplet near 1253 \AA is also detected in the Ly α forest, but it is strongly contaminated by the Ly α forest absorptions. By fitting the four dominant components (7, 8, 10 and 11), an upper limit to the $N(\text{S II})$ column density has been derived.

4. Relative abundances

4.1. Metallicity and dust content

The metallicity $[\text{Fe}/\text{H}] = -1.97 \pm 0.19$ of the most distant DLA system known to the present date at $z_{\text{abs}} = 4.466$, observed when the age of the universe was only 1.3^3

Gyr, is low but still a factor of two higher than the most metal-poor Galactic stars. It is not even the lowest metallicity level of all known DLA systems. Several systems have metallicities much lower than that and some of them in fact do lie at $z_{\text{abs}} < 3$. The lowest abundances known to date, $[\text{Fe}/\text{H}] < -2.6$, have been measured at $z_{\text{abs}} = 2.076$ toward Q 2206–199 (Prochaska & Wolfe 1997a), at $z_{\text{abs}} = 2.618$ toward Q 0913+072 (Ledoux et al. 1998) and at $z_{\text{abs}} = 4.203$ toward BR 0951–04 (Prochaska & Wolfe 1999). The $[\text{Fe}/\text{H}] = -1.97 \pm 0.19$ value of this system indeed shows that the very young object (≤ 1.3 Gyr) responsible for the DLA absorber has already experienced a significant metal production.

Prochaska & Wolfe (2000) have recently discussed the high-quality measurements of the Fe abundance in 39 DLA systems. They find a moderate trend (with a large scatter) of decreasing $[\text{Fe}/\text{H}]$ for individual absorbers from $z_{\text{abs}} = 1.5$ to 4.4. The $N(\text{H I})$ -weighted mean metallicity exhibits on the contrary a minimal evolution over the same redshift interval. Our result at $z_{\text{abs}} = 4.466$ is consistent with this recent metallicity evolution review, since the metallicity found, $[\text{Fe}/\text{H}] = -1.97 \pm 0.19$, is representative of the unweighted mean $[\text{Fe}/\text{H}]$ metallicity for their high-redshift sub-sample, $\langle [\text{Fe}/\text{H}] \rangle_{z_{\text{high}}=[3;4.4]} = -1.83$.

The estimated upper limit of the nickel abundance $[\text{Ni}/\text{H}] < -2.35$ gives $[\text{Ni}/\text{Fe}] < -0.41$. This upper limit is significantly lower than the $[\text{Ni}/\text{Fe}]$ values found in Galactic metal-poor stars which are nearly solar down to very low metallicities (Goswami & Prantzos 2000). This underabundance of $[\text{Ni}/\text{Fe}]$, measured despite the use of the updated Ni II f -value from Zsargó & Ferderman (1998), may be interpreted at a first glance as the result of differential depletion of Ni and Fe from the gas phase onto dust grains by analogy to what is observed in the Galactic ISM with Ni being more heavily depleted than Fe (Savage & Sembach 1996). However, this interpretation has to be considered

² $[\text{X}/\text{H}] \equiv \log[N(\text{X})/N(\text{H})]_{\text{DLA}} - \log[N(\text{X})/N(\text{H})]_{\odot}$.

³ Assuming $H_0 = 60 \text{ km s}^{-1} \text{ Mpc}^{-1}$, $\Omega_0 = 0.4$, $\Lambda_0 = 0.6$.

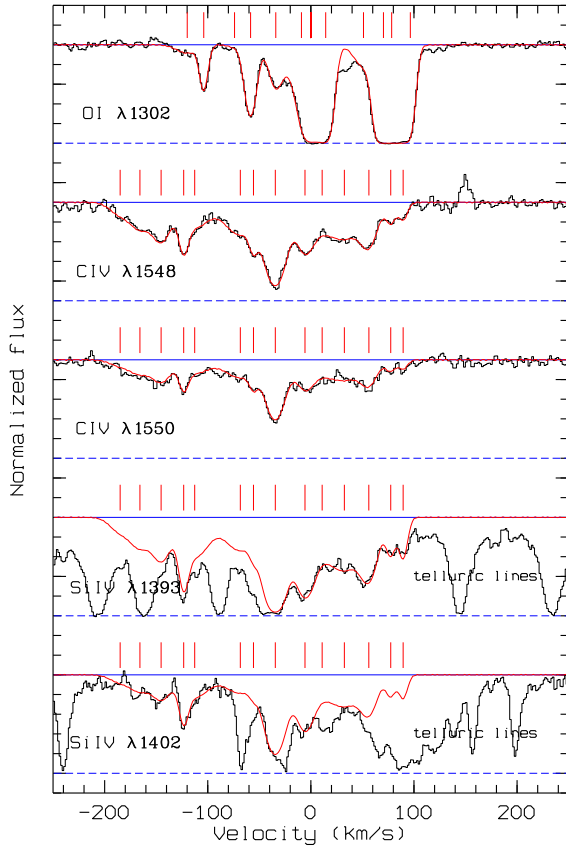


Fig. 2. Absorption-line profiles of the high-ion transition plotted against velocity for the DLA system at $z_{\text{abs}} = 4.466$. The vertical scale goes from 0 to 1 for each plotted line transition. The zero velocity is fixed at $z = 4.466582$. The vertical bars mark the positions of the 14 velocity components as given in Table 3. The thin solid curve represents the best fit solution. The Si IV $\lambda\lambda 1393, 1402$ lines are partly blended with telluric absorption lines. The O I profile is plotted in order to facilitate the comparison between low- and high-ion profiles.

with caution, since the measurement of Ni in the dust-free DLA system toward Q 0000–2620 by Molaro et al. (2000) shows also a significant underabundance of [Ni/Fe], [Ni/H] = -2.27 for a metallicity of [Fe/H] = -2.04 . Thus, the [Ni/Fe] ratio is not a good indicator of dust content in DLA systems.

The best constraint on dust content we have for the DLA system at $z_{\text{abs}} = 4.466$ comes from the nearly solar [O/Si] ratio of -0.09 ± 0.18 . It is suggestive of limited amounts of dust, since O is a non-refractory element and a depletion of Si onto dust grains would imply an intrinsic [O/Si] ratio much too undersolar. The derived [O/Si] ratio is also in excellent agreement with the usual assumption of nearly solar [O/ α] ratios in DLA systems (e.g. Lu et al. 1998). Limited amounts of dust in this DLA system allow a study of relative abundances exempt from strong uncer-

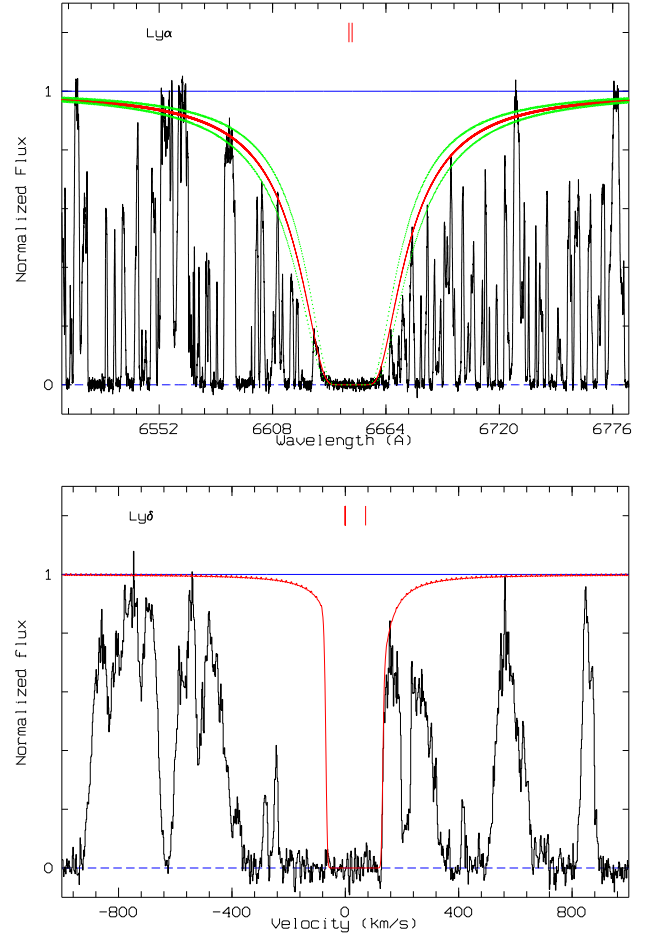


Fig. 3. Damped Ly α and Ly δ absorption profiles plotted against vacuum heliocentric wavelength (*top*) and velocity (*bottom*) for the DLA system at $z_{\text{abs}} = 4.466$. The vertical bars mark the positions of 2 stronger components (7 and 11) at $z = 4.466582$ and $z = 4.468005$. The thin solid curve represents the best fit of the damping profile with $N(\text{H I}) = 1.07 \times 10^{20} \text{ cm}^{-2}$, $b = 20.0 \text{ km s}^{-1}$ and $N(\text{H I}) = 3.63 \times 10^{20} \text{ cm}^{-2}$, $b = 16.5 \text{ km s}^{-1}$ (respectively). The light dotted curves are damping profiles with $N(\text{H I}) = (0.86, 2.90) \times 10^{20} \text{ cm}^{-2}$ and $N(\text{H I}) = (1.28, 4.36) \times 10^{20} \text{ cm}^{-2}$ (respectively).

tainties deriving from the unknown fraction of elements which condenses onto dust grains.

4.2. α -element to Fe abundances

The [α /Fe] abundance ratio is a good indicator of the chemical evolution history which can be used to understand the nature of galaxies. In the early stages of the chemical evolution of galaxies the abundances are likely dominated by Type II supernovae (SNe) products rich in α -elements created within $< 2 \times 10^7$ yr. The Type

Table 4. Ionic column densities and relative abundances for the DLA system at $z_{\text{abs}} = 4.466$

Ion	λ_{rest}	f	$\log N^c$	$[\text{X}/\text{H}]^f$
H I....	1215.670 ^a	0.41640 ^a	20.67 ± 0.09	...
C II....	1334.532 ^a	0.12780 ^a	> 15.59	> -1.63
C II*..	1335.708 ^a	0.11490 ^a	< 13.59	...
C IV... 1550.770 ^a	1548.195 ^a 0.09522 ^a	0.19080 ^a ...	14.27 ± 0.06
N I.... 1200.223 ^a 1200.710 ^a	1199.550 ^a 0.13280 ^a 0.04423 ^a	0.13280 ^a 0.08849 ^a ...	13.57 ± 0.12	-3.07 ± 0.15
O I.... 1039.230 ^a 936.629 ^a	1302.168 ^a 0.04887 ^a 0.00920 ^a 0.00314 ^a	0.04887 ^a 0.00920 ^a ...	15.91 ± 0.17	-1.63 ± 0.19
Al II... Si II... 1526.707 ^b	1670.787 ^a 1304.370 ^b 0.11000 ^b	1.83300 ^a 0.08600 ^b ...	13.36 ± 0.06 14.68 ± 0.07 ...	-1.79 ± 0.11 -1.54 ± 0.11 ...
Si IV... 1402.770 ^a	1393.755 ^a 0.51400 ^a 0.25530 ^a	0.51400 ^a ...	14.09 ± 0.12
S II.... 1253.811 ^a 1259.519 ^a	1250.584 ^a 0.00545 ^a 0.01088 ^a 0.01624 ^a	0.00545 ^a	< 15.46	< -0.41
Fe II... Ni II... 1370.132 ^d	1608.451 ^c 1314.217 ^d 0.14400 ^d	0.06196 ^c 0.14580 ^d ...	14.21 ± 0.17 < 12.60 < 12.57	-1.97 ± 0.19 < -2.35 ...

^a From Morton 1991.^b From Spitzer & Fitzpatrick 1993.^c From Cardelli & Savage 1995.^d From Zsargó & Federman 1998.^e Column density from line profile fitting. Upper limits are 4σ .^f Abundance relative to the solar value of Grevesse et al. 1996.

I SNe products, the Fe-peak elements, entered into the game only after $> 10^8 - 10^9$ yr. Thus, in the early stages the α -elements are expected to be more abundant than the Fe-peak elements, and the ratio $[\alpha/\text{Fe}]$ should decline later on during evolution. The exact timing of the decline depends on both the star formation rate and the initial mass function. A galaxy which turns most of its gas into stars within 10^9 yr would maintain an enhanced $[\alpha/\text{Fe}]$ ratio while $[\text{Fe}/\text{H}]$ grows to high values (Fuhrmann 1998). At the other extreme, in a galaxy with a small star formation rate or with bursts separated by quiescent periods lasting more than 10^9 yr, there would be time for $[\alpha/\text{Fe}]$ to decline to at least solar values while $[\text{Fe}/\text{H}]$ remains low (Pagel & Tautvaisviene 1998).

Si is the most accessible α -element in the DLA systems. However it is a refractory element, and due to the Si depletion coupled with a stronger Fe depletion onto dust grains (Savage & Sembach 1996), we observe similar $[\text{Si}/\text{Fe}]$ ratios in the Galactic interstellar medium (ISM) as in the Galactic metal-poor stars presumed to exhibit nucleosynthetic patterns typical of Type II supernovae. In the presence of dust, it is therefore difficult to deter-

mine the intrinsic $[\text{Si}/\text{Fe}]$ enhancement. In the DLA system at $z_{\text{abs}} = 4.466$, we derive $[\text{Si}/\text{H}] = -1.54 \pm 0.11$ which implies $[\text{Si}/\text{Fe}] = 0.43 \pm 0.18$, a relatively high α enhancement. At the metallicity of $[\text{Fe}/\text{H}] = -1.97 \pm 0.19$, this $[\text{Si}/\text{Fe}]$ value corresponds to the typical values of the Galactic metal-poor stars (Goswami & Prantzos 2000), and in a dust-limited system it is suggestive of a Type II SN enrichment.

Oxygen is also a typical product of Type II SNe and shows an important enhancement in Galactic metal-poor stars, $[\text{O}/\text{Fe}] \simeq 0.35$ at $[\text{Fe}/\text{H}] = -2.00$ (McWilliam 1997). Claims for an even more extreme overabundance of O with $[\text{O}/\text{Fe}]$ reaching 1.0 dex at $[\text{Fe}/\text{H}] = -3.0$ have recently been made by Israelian et al. (1998) and Boesgaard et al. (1999). The oxygen dust depletion is negligible (Savage & Sembach 1996), therefore O is an excellent diagnostic tool of the $[\alpha/\text{Fe}]$ abundance ratio. In the studied DLA system, we derive $[\text{O}/\text{H}] = -1.63 \pm 0.19$, which implies $[\text{O}/\text{Fe}] = 0.34 \pm 0.24$. This value is representative of the typical Type II SN enriched Galactic metal-poor star abundance pattern.

Another important diagnostic tool of the $[\alpha/\text{Fe}]$ abundance ratio is sulphur. S also shows in Galactic metal-poor stars the typical enhancement of α -elements with $[\text{S}/\text{Fe}] \simeq 0.4/0.6$ (François 1988), and it is nearly undepleted from gas to dust (Savage & Sembach 1996). We manage to derive only a non-significant upper limit $[\text{S}/\text{H}] < -0.41$, which does not provide any interesting constraint on the $[\text{S}/\text{Fe}]$ ratio ($[\text{S}/\text{Fe}] < 1.56$).

We have finally at our disposal essentially two indicators of the α -element abundances, Si and O. The $[\text{Si}/\text{Fe}] = 0.43 \pm 0.18$ and $[\text{O}/\text{Fe}] = 0.34 \pm 0.24$ ratios both show a significant $[\alpha/\text{Fe}]$ enhancement due to the Type II SN enrichment similar to that of the Galactic stars with comparable metallicities. A $[\alpha/\text{Fe}]$ enhancement due to dust depletion effects is ruled out by the presence of limited amounts of dust in this DLA system. We can thus suggest that the DLA system towards APM BR J0307–4945 is undergoing a chemical evolution enrichment similar to that expected in the initial phases of a massive galaxy like the Milky Way.

4.3. Nitrogen abundance

Nitrogen is a key element in understanding the evolution of galaxies with few star forming events, since it needs relatively long timescales as well as relatively high underlying metallicity to be produced (Matteucci et al. 1997). The reason is that N is believed to be produced principally in intermediate-mass stars, specifically those stars between 4 and $8 M_{\odot}$ which undergo hot bottom burning and expel large amounts of primary N at low metallicities and secondary N at higher metallicities produced in the CNO cycle from C and O created in earlier generations of stars (Henry et al. 2000).

In our system the N abundance is $[\text{N}/\text{H}] = -3.07 \pm 0.15$, which implies $[\text{N}/\text{O}] = -1.44 \pm 0.21$ at $[\text{O}/\text{H}] = -1.63 \pm 0.19$. This very low $[\text{N}/\text{O}]$ ratio, much lower than the corresponding values in the Milky Way and in the H II regions, lies in the region limited by the tracks of primary and secondary N production (Vila-Costas & Edmunds 1993), close to a pure secondary N production behaviour.

All studied DLA systems occupy the same delimited region, and show a large scatter with some $[\text{N}/\text{O}]$ values consistent with a pure secondary behaviour and others requiring a primary production of N (Lu et al. 1998, Centurión et al. 1998). The different $[\text{N}/\text{O}]$ values observed at a given $[\text{O}/\text{H}]$ may be interpreted in terms of the delayed delivery of N with respect to O when star formation proceeds in bursts (Edmunds & Pagel 1978). In this model, galaxies that have experienced a recent episode of star formation show low $[\text{N}/\text{O}]$ ratios due to the quick production of O in massive stars (~ 6 Myr for a $25 M_{\odot}$ star). Galaxies that have been quiescent for a long period show high $[\text{N}/\text{O}]$, N is released after approximately 250 Myr as a product of intermediate-mass stars and the $[\text{N}/\text{O}]$ ratio increases while $[\text{O}/\text{H}]$ remains constant. Therefore, the scatter comes about by observing DLA systems in various stages of O and N enrichment.

The derived very low $[\text{N}/\text{O}]$ ratio may thus be explained as representing very early stages of N/O evolution when intermediate-mass stars have not yet begun to release N, i.e. roughly 250 Myr or less after a star burst. It thus seems reasonable to expect also an overabundance of the α -elements relative to Fe-peak elements, an overabundance which has been highlighted by the $[\text{Si}/\text{Fe}]$ and $[\text{O}/\text{Fe}]$ abundance ratios in Sect. 4.2.

5. Kinematics

The metal line profiles of DLA absorbers in principle provide information in velocity space on the gas kinematics. Whether this information can be used as a diagnostic of motions on galactic scales and what motions indeed dominate the kinematics is still an open question. The kinds of motion one may expect to be at play in a gas-rich environment, and in proto-galaxies, are rotation of clouds in a disk-like structure, and radial infall and random motions of clouds in a halo. A realistic description may have to combine both effects as is probably the case in Mg II and Lyman-limit systems at intermediate redshifts (Charlton & Churchill 1996). In DLA systems, systematic high-resolution studies of low-ionization lines have established that the profiles are often asymmetric with the strongest absorption lying at an edge of the profile (Prochaska & Wolfe 1997b, 1998). This was first interpreted as the signature of large, fast-rotating thick disks although the current body of data is also consistent with relative motions of clouds with limited rotation (Haehnelt et al. 1998, Ledoux et al. 1998, McDonald & Miralda-Escudé 1999).

In the DLA absorber towards APM BR J0307–4945, the shape of the unsaturated Fe II $\lambda 1608$ line profile is strongly suggestive of edge-leading asymmetry in the sense that the strongest absorption itself is located at an edge of the profile (see Fig. 1). The signal-to-noise ratio is not high enough in this spectral region, however, to decide whether the entire profile is asymmetric, with steadily decreasing optical depth with decreasing wavelength. Stronger transition lines from different elements including Al II and O I, the latter being a good tracer of the neutral phase, indeed display huge variations of optical depths along their profiles. In particular, whereas the low-ion profiles extend over 240 km s^{-1} , they have relatively small or negligible optical depths in a spectral region 25 km s^{-1} wide just blueward of the strong components at the red edge of the profiles. Moreover, the best fit model described in Sect. 3 indeed indicates that about 80% of the metals are distributed in two sub-systems of comparable importance, separated by $\sim 70 \text{ km s}^{-1}$ and spanning only about 25 km s^{-1} each (components 6, 7, 8 on the one hand, and 10, 11, 12 on the other hand). The kinematics of the absorber can therefore also be understood as having a main double peaked structure. This is expected, for instance, during a merging event involving two proto-galactic clumps surrounded by tidal material and radially infalling clouds; this possibility is strongly supported by the results of numerical N-body/hydrodynamic simulations (see Haehnelt et al. 1998, 2000).

The comparison of the relative strength and velocity distribution of line profiles arising from different phases also provides information on the ionization structure and spatial distribution of the absorbing gas. In the DLA system under study, the shapes of the C IV and Si IV profiles are similar and globally symmetric with the strongest absorption located at the center of the profile; they also clearly differ from the low ions. The total velocity broadening is larger for the high-ion (305 km s^{-1}) than it is for the low-ion profiles (240 km s^{-1}). However the two different phases are related, it has been shown from a statistical point of view that there is a trend for the total velocity broadenings of C IV and Fe II to be correlated (Ledoux et al. 1998; see also Wolfe & Prochaska 2000). Besides, it is apparent in Fig. 2 that, while there is a velocity interval common to both phases, the high-ion profiles extend much farther into the blue. The DLA absorber towards APM BR J0307–4945 may thus be a good illustration of a scenario in which ionized gas is flowing out with velocities of up to $\sim -300 \text{ km s}^{-1}$ relative to the bulk of one of two main neutral clumps.

6. Conclusion

Observations with the new UVES echelle spectrograph at the 8.2m VLT Kueyen telescope provided the first high-quality spectra of the distant APM BR J0307–4945 quasar at $z_{\text{em}} = 4.73$. We focused our analysis on the

metal abundances of a damped Ly α system at $z_{\text{abs}} = 4.466$, the most distant DLA system known to the present date, observed when the age of the universe was only 1.3 Gyr. It has a hydrogen column density of $N(\text{H I}) = (4.68 \pm 0.97) \cdot 10^{20} \text{ cm}^{-2}$, and shows complex low- and high-ion line profiles spanning ≈ 240 and 300 km s^{-1} in velocity space respectively. By fitting Voigt profiles to the observed absorption lines and by neglecting ionization corrections, we obtained $[\text{N}/\text{H}] = -3.07 \pm 0.15$, $[\text{O}/\text{H}] = -1.63 \pm 0.19$, $[\text{Al}/\text{H}] = -1.79 \pm 0.11$, $[\text{Si}/\text{H}] = -1.54 \pm 0.11$, $[\text{Fe}/\text{H}] = -1.97 \pm 0.19$, and we placed a lower limit on the abundance of C, $[\text{C}/\text{H}] > -1.63$ and an upper limit on the abundance of Ni, $[\text{Ni}/\text{H}] < -2.35$.

The Fe abundance, $[\text{Fe}/\text{H}] = -1.97 \pm 0.19$, is representative of the mean $[\text{Fe}/\text{H}]$ metallicity (unweighted by the H I column density) for the high-redshift sub-sample of Prochaska & Wolfe (2000), and is thus consistent with a moderate metallicity decrease towards high redshifts. This metallicity, $\sim 1/90$ solar, also shows that the very young object (≤ 1.3 Gyr) responsible for the DLA absorber has already experienced a significant metal enrichment.

The relative $[\alpha/\text{Fe}]$ abundance ratios resemble those expected in the early phases of evolution of a massive galaxy such as our own Galaxy. The $[\text{Si}/\text{Fe}] = 0.43 \pm 0.18$ and $[\text{O}/\text{Fe}] = 0.34 \pm 0.24$ ratios indeed show both a significant $[\alpha/\text{Fe}]$ enhancement due to Type II SN enrichment similar to the one of the Galactic stars with comparable metallicities, in the presence of limited amounts of dust as inferred by the nearly solar $[\text{O}/\text{Si}]$ ratio. The Type II SN enrichment is further supported by the very low $[\text{N}/\text{O}] = -1.44 \pm 0.21$ ratio.

Acknowledgements. We are indebted to all people involved in the conception, construction and commissioning of UVES for the high quality of the spectra obtained early in the operation of the instrument. We warmly thank J.X. Prochaska and J. Bergeron for useful comments on an earlier version of the paper and P. Bristow for carefully checking the english text. M.D.-Z. is supported by an ESO Studentship and the Swiss National Funds.

References

- Boesgaard A.M., King J.R., Deliyannis C.P., Vogt S.S., 1999, AJ 117, 492
- Cardelli J.A., Savage B.D., 1995, ApJ 452, 275
- Centurion M., Bonifacio P.B., Molaro P., Vladilo G., 1998, ApJ 509, 620
- Charlton J.C., Churchill C.W., 1996, ApJ 465, 631
- Dekker H., D’Odorico S., Kaufer A., Delabre B., Kotzlowski H., 2000, Proceedings of the SPIE Conference 4008, 534
- D’Odorico S., Cristiani S., Dekker H., Hill V., Kaufer A., Kim T.-S., Primas F., 2000, Proceedings of the SPIE Conference 4005, in press
- Edmunds M.G., Pagel B.E.J., 1978, MNRAS 185, 78
- Fontana A., Ballester P., 1995, The Messenger 80, 37
- François P., 1988, A&A 195, 226
- Fuhrmann K., 1998, A&A 338, 161
- Goswami A., Prantzos N., 2000, A&A 359, 191
- Grevesse N., Noels A., Sauval A.J., 1996, Astron. Society of the Pacific Conf. Series, vol. 99, 117
- Haehnelt M.G., Steinmetz M., Rauch M., 1998, ApJ 495, 647
- Haehnelt M.G., Steinmetz M., Rauch M., 2000, ApJ 534, 594
- Henry R.B.C., Edmunds M.G., Köppen J., 2000, ApJ 541, 660
- Israelian G., Garcia Lopez R., Rebolo R., 1998, ApJ 507, 805
- Lanzetta K.M., Wolfe A.M., Turnshek D.A., 1995, ApJ 440, 435
- Le Brun V., Bergeron J., Boisse P., Deharveng J. M., 1997, A&A 321, 733
- Ledoux C., Petitjean P., Bergeron J., Wampler E.J., Srianand R., 1998, A&A 337, 51
- Lu L., Savage B.D., Tripp T.M., Meyer D.M., 1995, ApJ 447, 597
- Lu L., Sargent W.L.W., Barlow T.A., Churchill C.W., Vogt S.S., 1996, ApJS 107, 475
- Lu L., Sargent W.L.W., Barlow T.A., 1997, astro-ph/9711298
- Lu L., Sargent W.L.W., Barlow T.A., 1998, AJ 115, 55
- Matteucci F., Molaro P., Vladilo G., 1997, A&A 321, 45
- McDonald P., Miralda-Escudé J., 1999, ApJ 519, 486
- McMahon R.G. et al., 2001, in preparation
- McWilliam A., 1997, ARA&A 35, 503
- Molaro P., Bonifacio P., Centurion M., D’Odorico, S. Vladilo, G. Santin, P., Di Marcantonio P., 2000, ApJ 541, 54
- Morton D.C., 1991, ApJS 77, 119
- Pagel B.E.J., Tautvaisiene G., 1998, MNRAS 299, 535
- Péroux C., Storrie-Lombardi L.J., McMahon R.G., Irwin M., Hook I.M., 2001, astro-ph/0101179
- Pettini M., Smith L.J., King D.L., Hunstead R.W., 1997, ApJ 486, 665
- Pettini M., 2000, Philosophical Transactions of the Royal Society of London, Series A, Vol. 358, no. 1772, 203
- Prochaska J.X., Wolfe A.M., 1997a, ApJ 474, 140
- Prochaska J.X., Wolfe A.M., 1997b, ApJ 487, 73
- Prochaska J.X., Wolfe A.M., 1998, ApJ 507, 113
- Prochaska J.X., Wolfe A.M., 1999, ApJS 121, 369
- Prochaska J.X., Wolfe A.M., 2000, ApJ 533, L5
- Rao S.M., Turnshek D.A., 2000, ApJS 130, 1
- Savage B.D., Sembach K.R., 1996, ARA&A 34, 279
- Spitzer L.J., Fitzpatrick E.L., 1993, ApJ 409, 299
- Storrie-Lombardi L.J., McMahon R.G., Irwin M., 1996, MNRAS 283, 79
- Storrie-Lombardi L.J., Wolfe A.M., 2000, ApJ 543, 552
- Storrie-Lombardi L.J., Irwin M.J., McMahon R.G., Hook I.M., 2001, MNRAS, submitted
- Viegas S.M., 1995, MNRAS 276, 268
- Vila-Costas M.B., Edmunds M.G., 1993, MNRAS 265, 199
- Wolfe A. M., Turnshek D. A., Smith H. E., Cohen R. D., 1986, ApJS 61, 249
- Wolfe A.M., Lanzetta K.M., Foltz C.B., Chaffee F.H., 1995, ApJ 454, 698
- Wolfe A.M., Prochaska J.X., 2000, ApJ 545, in press
- Zsargó J., Federman S.R., 1998, ApJ 498, 256

Table 5. Identified metal systems from absorption lines redwards of the Ly α emission for the quasar APM BR J0307–4945

λ_{vac} [Å]	W [Å]	Ident	z_{abs}	λ_{vac} [Å]	W [Å]	Ident	z_{abs}
6954.33	2.550 ± 0.074	C II λ 1334	4.211	8067.64	3.508 ± 0.273	C IV λ 1548	4.211
6964.28	0.987 ± 0.039	C II λ 1334	4.218	8078.48	5.708 ± 0.305	C IV λ 1548	4.218
7012.54	0.071 ± 0.008	Si IV λ 1393	4.031	8080.78	4.098 ± 0.428	C IV λ 1550	4.211
7107.39	0.968 ± 0.085	C IV λ 1548	3.591	8091.92	3.269 ± 0.428	C IV λ 1550	4.218
7118.51	3.106 ± 0.151	O I λ 1302	4.466	8113.90	0.080 ± 0.033	Ca II λ 3969	1.044
7130.40	2.364 ± 0.119	Si II λ 1304	4.466	8267.33	0.267 ± 0.107	?	
7139.90	0.288 ± 0.059	Ni II λ 1370	4.211	8302.34	0.282 ± 0.087		
7141.83	0.084 ± 0.017	?		8344.94	2.245 ± 0.316	Si II λ 1526	4.466
7142.57	0.080 ± 0.016	?		8436.70	0.144 ± 0.072	?	
7155.86	0.072 ± 0.023	?		8463.15	2.361 ± 0.304	C IV λ 1548	4.466
7167.68	0.050 ± 0.017	?		8477.34	1.484 ± 0.324	C IV λ 1550	4.466
7177.07	0.086 ± 0.027	?		8506.34	0.321 ± 0.041	Fe II λ 2344	2.629
7264.03	3.505 ± 0.158	Si IV λ 1393	4.211	8508.96	0.430 ± 0.052	Fe II λ 2344	2.630
7273.05	3.538 ± 0.258	Si IV λ 1393	4.218	8616.15	0.125 ± 0.041	Fe II λ 2374	2.629
7283.88	0.177 ± 0.075			8618.75	0.167 ± 0.042	Fe II λ 2374	2.630
7294.96	4.562 ± 0.275	C II λ 1334	4.466	8646.29	0.641 ± 0.073	Fe II λ 2382	2.629
7309.88	2.831 ± 0.178	Si IV λ 1402	4.211	8648.86	0.820 ± 0.082	Fe II λ 2382	2.630
7320.09	1.930 ± 0.262	Si IV λ 1402	4.218	8650.44	0.388 ± 0.085	C IV λ 1548	4.587
7347.91	0.154 ± 0.043	C IV λ 1548	3.746	8654.34	0.079 ± 0.055	C IV λ 1548	4.590
7360.07	0.053 ± 0.034	C IV λ 1550	3.746	8662.13	0.067 ± 0.024		
7370.40	0.578 ± 0.051	C IV λ 1548	3.760	8664.78	0.297 ± 0.093	C IV λ 1550	4.587
7382.67	0.379 ± 0.054	C IV λ 1550	3.760	8668.66	0.090 ± 0.046	C IV λ 1550	4.590
7384.58	0.830 ± 0.085	Fe II λ 1608	3.591	8686.18	0.455 ± 0.127	C IV λ 1548	4.610
7470.32	0.711 ± 0.102	C IV λ 1548	3.825	8700.80	0.200 ± 0.127	C IV λ 1550	4.610
7482.75	0.428 ± 0.099	C IV λ 1550	3.825	8706.55	0.754 ± 0.199	Al II λ 1670	4.211
7618.87	<i>blended*</i>	Si IV λ 1393	4.466	8719.02	0.435 ± 0.234	Al II λ 1670	4.218
7668.13	<i>blended*</i>	Si IV λ 1402	4.466	8775.55	0.086 ± 0.047	?	
7670.75	1.971 ± 0.128	Al II λ 1670	3.591	8791.73	0.906 ± 0.289	Fe II λ 1608	4.466
7748.87	0.048 ± 0.032	?		8794.97	0.319 ± 0.053	?	
7785.87	0.056 ± 0.024	?		9132.58	2.581 ± 0.366	Al II λ 1670	4.466
7787.36	0.172 ± 0.056	Si IV λ 1393	4.587	9152.38	0.065 ± 0.050	?	
7789.51	0.133 ± 0.041	C IV λ 1548	4.031	9197.92	0.098 ± 0.046	?	
7791.05	0.061 ± 0.036	Si IV λ 1393	4.590	9386.06	0.276 ± 0.078	Fe II λ 2586	2.629
7802.54	0.079 ± 0.036	C IV λ 1550	4.031	9389.16	0.829 ± 0.196	Fe II λ 2586	2.630
7837.81	0.046 ± 0.025	Si IV λ 1402	4.587	9416.03	0.080 ± 0.062	?	
7841.41	0.031 ± 0.021	Si IV λ 1402	4.590	9435.16	0.587 ± 0.088	Fe II λ 2600	2.629
7955.78	0.714 ± 0.140	Si II λ 1526	4.211	9437.99	0.676 ± 0.121	Fe II λ 2600	2.630
7967.11	0.420 ± 0.304	Si II λ 1526	4.218	9489.26	0.166 ± 0.095		
8042.74	0.139 ± 0.046	Ca II λ 3934	1.044				

* Line profiles contaminated by telluric lines; ? Unidentified